

Nanotube heat conductors under tensile strain: Reducing the three-phonon scattering strength of acoustic phonons

Daniel Bruns,^{1,2,*} Alireza Nojeh,^{3,2} A. Srikantha Phani,⁴ and Jörg Rottler^{1,2}

¹*Department of Physics and Astronomy, University of British Columbia, Vancouver, BC, Canada V6T 1Z1*

²*Quantum Matter Institute, University of British Columbia, Vancouver, BC, Canada V6T 1Z4*

³*Department of Electrical and Computer Engineering,*

University of British Columbia, Vancouver, BC, Canada V6T 1Z4

⁴*Department of Mechanical Engineering, University of British Columbia, Vancouver, BC, Canada V6T 1Z4*

(Dated: August 25, 2021)

Acoustic phonons play a special role in lattice heat transport, and confining these low-energy modes in low-dimensional materials may enable nontrivial transport phenomena. By applying lowest-order anharmonic perturbation theory to an atomistic model of a carbon nanotube, we investigate numerically and analytically the spectrum of three-phonon scattering channels in which at least one phonon is of low energy. Our calculations show that acoustic longitudinal (LA), flexural (FA), and twisting (TW) modes in nanotubes exhibit a distinct dissipative behavior in the long-wavelength limit, $|k| \rightarrow 0$, which manifests itself in scattering rates that scale as $\Gamma_{\text{LA}} \sim |k|^{-1/2}$, $\Gamma_{\text{FA}} \sim k^0$, and $\Gamma_{\text{TW}} \sim |k|^{1/2}$. These scaling relations are a consequence of the harmonic lattice approximation and critically depend on the condition that tubes are free of mechanical strain. In this regard, we show that small amounts of tensile lattice strain ϵ reduce the strength of anharmonic scattering, resulting in strain-modulated rates that, in the long-wavelength limit, obey $\Gamma \sim \epsilon^r |k|^s$ with $r \leq 0$ and $s \geq 1$, irrespectively of acoustic mode polarization. Under the single-mode relaxation time approximation of the linearized Peierls-Boltzmann equation (PBE), the long-tube limit of lattice thermal conductivity in stress-free and stretched tube configurations can be unambiguously characterized. Going beyond relaxation time approximations, analytical results obtained in the present study may help to benchmark numerical routines which aim at deriving the thermal conductivity of nanotubes from an exact solution of the PBE.

I. INTRODUCTION

Two-dimensional graphene sheets and their one-dimensional derivatives, carbon nanotubes, exhibit an extremely efficient lattice heat transport [1, 2]. While the merits of integrating these carbon allotropes into thermal management applications have been convincingly demonstrated in recent years [3–8], separating their intrinsic low-dimensional heat transport properties from external factors remains a challenge [9, 10]. Residual strain in the carbon lattice is commonly identified as one source of measurement uncertainty among others in heat transport experiments involving nanostructured carbon samples [9, 10]. A thorough understanding on theoretical grounds of the role of strain in low-dimensional lattice heat transport is therefore crucial.

Focusing on the effects of strain in lattice heat transport, phonon frequencies in three-dimensional crystals are typically described by a positive mode-specific Grüneisen parameter [11, 12], which translates to frequency hardening of phonons under compressive and softening under tensile loading. Roughly speaking, an overall downward shift of frequencies under a tensile load leads to a reduction of phonon group velocities, which in turn causes a reduced rate of lattice heat transfer. Even though other phonon properties play a role as

well, such a qualitative trend was generally confirmed for three-dimensional systems [13]. In contrast, one and two-dimensional crystals allow for atomic out-of-line and out-of-plane vibrations, respectively, whose associated phonon frequencies instead harden under tensile strain [12, 14]. In light of these *flexural* modes, nonconventional strain behavior of low-dimensional heat transport in graphene and carbon nanotubes might be anticipated.

The linearized Peierls-Boltzmann equation (PBE) for phonon transport has become a standard tool to tackle anharmonic phonon interactions and the emergence of thermal resistivity in crystalline solids [15]. Within this formalism, determining the kinematically allowed three-phonon processes and their corresponding scattering amplitudes, as prescribed by anharmonic perturbation theory, is a key requirement for predicting the thermal conductivity. Bonini et al. [16] studied graphene in the framework of the PBE, making the notable observation that anharmonic scattering processes including acoustic flexural modes become systematically weakened under increasing tensile lattice strain. Specifically, by examining analytically the implications of anharmonic perturbation theory in the limit of low phonon energies, it was shown in Ref. [16] that the per-phonon conductivity contributions of weakly damped flexural modes under strain might grow without bound in the limit of large crystalline domain sizes. Although these conclusions with respect to thermal transport in graphene were later called into question and attributed to an inadequacy of relaxation

* dbruns@phas.ubc.ca

time approximations to the PBE [17, 18], the results in Ref. [16], nevertheless, give an unequivocal demonstration of the importance of lattice strain as far as low-frequency phonon scattering rates are concerned.

In the case of carbon nanotubes, some analytical considerations of three-phonon scattering rates were first presented by Mingo and Broido [19]. By simplifying the exact scattering formulas inherent to anharmonic perturbation theory, they derived approximate long-wavelength scaling relations capturing the three-phonon scattering strength of acoustic phonons, and thereby pointed out the issue of heat carrying modes with vanishing scattering rates. Later, more refined heat transport calculations within the PBE framework were performed on free-standing carbon nanotubes by us [20] and others [21–24]. With the help of numerical routines, these studies retained the full complexity associated with the many-body problem of interacting phonons, but did not account for the *exact* long-wavelength scaling relations of acoustic phonon scattering rates which are prescribed by lowest-order anharmonic perturbation theory. More so, to the best of our knowledge, the effects of strain on low-frequency three-phonon scattering rates involving flexural out-of-line vibrations have so far not been rigorously addressed within the PBE formalism.

To shed light on the manifestations of strain in lattice heat transport under one-dimensional phonon confinement, we examine here the case of carbon nanotubes in stress-free and stretched configurations. In particular, in anticipation of anomalous strain behavior rooted in the dynamics of flexural acoustic phonons [16], we put our emphasis on examining the three-phonon scattering amplitudes of nanotubes in the low-frequency limit. To this end, we carry out lattice-dynamical calculations which allow us to produce some general long-wavelength scaling relations resulting from lowest-order anharmonic perturbation theory, which are demonstrated to depend crucially on both tensile lattice strain as well as acoustic mode polarization. Importantly, while previous studies on stress-free nanotubes [20–24] resorted exclusively to reporting numerical results, here we support our data with an exact analysis of the behavior of three-phonon scattering rates in the low-frequency limit. As we show, earlier continuum modeling efforts on nanotubes [25–28] can, in part, help put numerical lattice-dynamical findings on firm theoretical footing. In this way, at the level of the single-mode relaxation time approximation to the PBE, unambiguous qualitative trends of the thermal conductivity in the long-tube limit can be given for both unstrained and stretched tube configurations.

This paper is structured as follows. In Sec. II, we give a brief account of our lattice-dynamical model and the numerical treatment of three-phonon interactions, with further computational details deferred to Appendix A. Section III establishes relevant links to continuum theories. Strain dependent scattering rates of acoustic phonons are presented in Sec. IV, and are complemented with exact long-wavelength scaling laws derived in Appendix B.

In Sec. V, these findings are applied to predict thermal conductivity coefficients of pristine tubes under a relaxation time approximation to the PBE. We finally discuss further research directions in Sec. VI and conclude in Sec. VII.

II. LATTICE-DYNAMICAL CALCULATIONS

To model carbon nanotubes, throughout this work we adopt a Tersoff type atomic interaction potential devised for sp²-hybridized carbon [29]. Rather than aiming at precise quantitative predictions accounting for tube chirality effects, our focus lies on finding generic trends of acoustic mode interactions in light of one-dimensional phonon confinement and tensile lattice strain. We therefore restrict our attention to isotropically pure nanotubes of chirality (4,4) with diameter $D \approx 5.55 \text{ \AA}$ and translational lattice parameter $a = (1 + \epsilon)a_0$, where $\epsilon \geq 0$ denotes a variable tensile strain amplitude and $a_0 \approx 2.51 \text{ \AA}$ corresponds to the tube's minimum-potential energy configuration in the stress-free state. Such achiral tubes of small diameter give rise to only a moderate number of phonon dispersion branches $\omega_j(k)$, in this case $j = 1, \dots, 48$. As a result, it is possible to consider the full spectrum of three-phonon scattering processes over a relatively fine wave number grid, spanning the one-dimensional Brillouin zone $-\pi/a < k \leq \pi/a$, which, as we show later, is crucial to resolve acoustic phonon dynamics in the long-wavelength limit $|k|a \ll 1$.

We calculate anharmonic phonon-phonon scattering rates within lowest-order perturbation theory. For a one-dimensional system, the total rate for a mode with polarization j and wave number k due to three-phonon interactions is derived, e.g., from the imaginary part of the phonon self-energy [30] and expressed as

$$\Gamma_j(k) = \frac{1}{N} \sum_{\substack{(k', j') \\ (k'', j'')}} \frac{1}{2} \Gamma_{jj'j''}^-(k, k', k'') + \Gamma_{jj'j''}^+(k, k', k''), \quad (1)$$

where N determines the grid spacing of wave numbers, $\Delta k = 2\pi/Na$, and the Γ^{\pm} 's describe three-phonon absorption (+) as well as decay (−) amplitudes. Introducing the shorthand $\nu = (j, k)$, individual transition amplitudes at finite temperature ($T > 0$) are given by

$$\Gamma_{\nu, \nu', \nu''}^{\pm} = \frac{\hbar\pi}{4\omega_{\nu}\omega_{\nu'}\omega_{\nu''}} \frac{(n_{\nu'} + 1/2 \pm 1/2)n_{\nu''}}{n_{\nu}} |V_{\nu, \nu', \nu''}^{\pm}|^2 \times \delta(\omega_{\nu} \pm \omega_{\nu'} - \omega_{\nu''}) \Delta_{k \pm k' - k'', 2\pi m/a}, \quad (2)$$

where the n_{ν} 's are the Bose-Einstein occupation numbers, $V_{\nu, \nu', \nu''}^{\pm} = V_{jj'j''}(k, \pm k', -k'')$ denote the Fourier transforms of the third order force constant tensor (see Appendix A), the delta function enforces energy conservation, and the discrete translational invariance of

the crystal lattice implies the conservation of quasimomentum as signified by the Kronecker delta Δ , with $m = 0$ and $m = \pm 1$ denoting normal and Umklapp scattering processes, respectively. Given the discrete rotational invariance of nanotubes, scattering processes are further subject to a quasiangular momentum selection rule [21, 31], which is not explicitly stated here but encoded in $V_{\nu,\nu',\nu''}^{\pm}$. Phonon triplets sampled from the same regular wave number grid generally cannot fulfill the condition of energy conservation and the delta function in Eq. (2) has to be resolved numerically. Here, we apply an adaptive Gaussian smearing approach [32] to compute phonon-phonon scattering rates as per Eqs. (1) and (2). Tensile lattice strain ϵ enters naturally into our calculations by influencing second and third order atomic force constants, which are the essential inputs to predict harmonic phonon spectra and three-phonon coupling coefficients $V_{jj'j''}$.

III. CONTINUUM MODELS AND ACOUSTIC PHONONS IN NANOTUBES

Treated as isotropic, free-standing, linear elastic continua, both long tubes and solid rods of radius R are known to permit three distinctive types of low-frequency waves: twisting (TW), longitudinal (LA) and two degenerate flexural bending (FA) type modes, exhibiting linear, $\omega_{\text{TW/LA}} \sim |k|$, and quadratic, $\omega_{\text{FA}} \sim Rk^2$, axial wave dispersion in the long-wavelength limit $|k|R \ll 1$ [33]. In the case of carbon nanotubes, these acoustic waves can be reproduced by a simple continuum model of a cylindrical surface [25, 26]. Specifically, by assuming that carbon nanotubes inherit the in-plane elastic isotropy of graphene sheets [25, 26], the acoustic wave dispersion for $|k| \rightarrow 0$ becomes

$$\begin{aligned} \omega_{\text{TW}}(k) &= v_{\text{TW}}|k|, & v_{\text{TW}} &= \sqrt{\frac{\mu}{\rho_m}}, \\ \omega_{\text{LA}}(k) &= v_{\text{LA}}|k|, & v_{\text{LA}} &= \sqrt{\frac{Y}{\rho_m}}, \\ \omega_{\text{FA}}(k) &= \frac{v_{\text{LA}}R}{\sqrt{2}}k^2, \end{aligned} \quad (3)$$

where the TW and LA wave velocities are determined by the 2D shear modulus μ , the 2D Young's modulus Y , and the area mass density of the cylinder surface ρ_m . More sophisticated continuum models have to be employed to account for tube chirality effects and elastic anisotropy. Considering both chiral and achiral tubes, recently, Gupta and Kumar [28] applied a Cosserat rod theory in order to derive analytical expressions for the acoustic wave dispersion under external loads. Following Ref. [28], to the lowest order in the tensile strain amplitude ϵ , frequency hardening of FA modes manifests itself in nanotubes as

$$\omega_{\text{FA}}^2(k, \epsilon) = \omega_{\text{FA}}^2(k, 0) + \mathcal{T}_1\epsilon k^2 - \mathcal{T}_2\epsilon k^4, \quad (4)$$

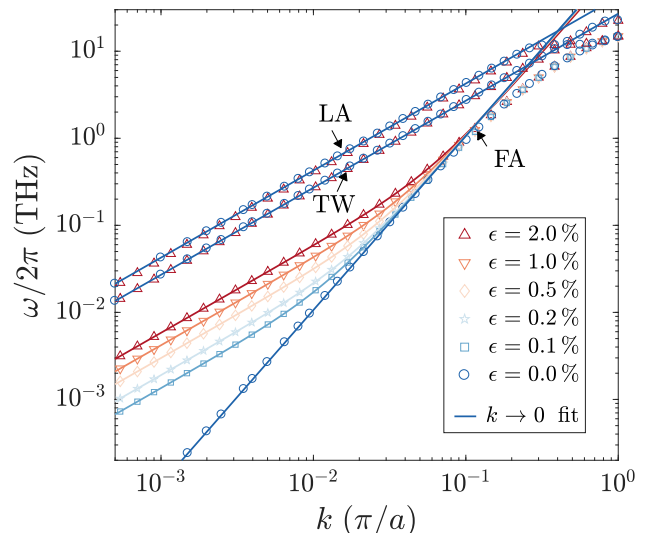


FIG. 1. Log-log plot of the acoustic phonon dispersion in (4,4) carbon nanotubes under varying tensile strain ϵ . Empty plot markers correspond to lattice-dynamical calculations that take strain dependent second order force constants as input. Solid lines are obtained by fitting the continuum predictions as per Eqs. (3) and (4) to phonon data in the region $k \leq 0.1 \pi/a$. Here, $\omega_{\text{TW}} = 27.04 k$, $\omega_{\text{LA}} = 42.56 k$ and $\omega_{\text{FA}}^2 = (10.61 - 73.70\epsilon) \times 10^3 k^4 + 1.75 \times 10^3 \epsilon k^2$ for twisting (TW), longitudinal (LA), and flexural (FA) modes, respectively, with ω_j in units of THz and k in units of π/a , where a denotes the lattice constant at a given strain amplitude.

where $\omega_{\text{FA}}(k, 0)$ denotes the FA mode dispersion in the stress-free state and the \mathcal{T}_i 's stand for some positive constants which relate to the tube's stretching and bending stiffness. For our model of a (4,4) carbon nanotube, acoustic mode frequencies obtained from lattice-dynamical calculations are plotted in Fig. 1. From TW and LA mode frequencies in unstrained tubes, we infer $v_{\text{TW}} = 13.57 \text{ km/s}$ and $v_{\text{LA}} = 21.37 \text{ km/s}$, respectively. At $\epsilon = 2.0\%$, TW mode velocities are found to be slightly increased by 0.2%, whereas LA mode velocities become smaller by 2.9%. Most importantly, under finite tensile strain, long-wavelength FA modes transition from a quadratic to a linear wave dispersion as is faithfully described by Eq. (4).

Continuum models might be further invoked to provide insight into acoustic phonon-phonon interaction processes. Within lowest-order perturbation theory, for a given acoustic phonon (j, k) of low energy and long wavelength, $\omega_j(|k| \rightarrow 0) = 0$, two types of interacting phonon triplets are permitted by the law of energy conservation: (i) triplets of three acoustic phonons, whose energies fall below the lowest optical phonon energy, $\omega_j \sim \omega_{j'} \sim \omega_{j''} \ll \omega_{\text{OPT}}$, or (ii) triplets of one acoustic and two optical modes, where $\omega_j \ll \omega_{\text{OPT}'} \sim \omega_{\text{OPT}''}$. A continuum approach lends itself to study scattering channels involving triplets of type (i). Treating stress-free carbon nanotubes as isotropic hollow cylinders and applying tools of nonlinear elasticity theory [34], it was shown by

De Martino et al. [27] that possible interacting acoustic mode triplets reduce to (LA, LA, LA), (LA, TW, TW), (LA, FA, FA), and (TW, FA, FA) for which coupling coefficients $V_{jj'j''}(k, k', k'')$ can be derived in terms of second and third order elastic constants. In particular, a noteworthy result of Ref. [27] is the quartic wave number dependence $V_{\text{TWFAFA}} \sim kk'k''(k' - k'')R$, which is at variance with the standard cubic long-wavelength approximation $V_{jj'j''} \sim kk'k''$ for type (i) triplets commonly found in classic textbooks [35, 36]. Within a lattice-dynamical treatment of three-phonon interactions, this behavior in carbon nanotubes was previously overlooked [21]. As we show below, the weak coupling strength between TW and FA modes gives rise to an intricate scattering behavior of low-frequency TW modes in stress-free and stretched tubes.

IV. ACOUSTIC MODE LEVEL ANALYSIS

Taking into account the full spectrum of three-phonon interactions including type (i) and (ii) phonon triplets, hereinafter, we evaluate acoustic phonon scattering rates within our lattice-dynamical model according to Eqs. (1) and (2) as a function of tensile strain ϵ . Specifically, in order to infer the governing long-wavelength scaling relations $\Gamma_j \sim \epsilon^r k^s$ for $j \in \{\text{LA, FA, TW}\}$, we decompose wave number-resolved scattering rates in the long-wavelength limit $0 < ka \ll 1$ into contributions that stem from individual three-phonon decay and absorption channels, $\Gamma_j = \sum_{j', j''} \Gamma_{jj'j''}^- / 2 + \Gamma_{jj'j''}^+$. For brevity in notation, mode polarizations appearing in triple subscripts are henceforth signified by single letters. For example, a triplet of type (ii) involving LA modes will be represented by LOO.

A. Longitudinal modes

Given the large group velocity of LA modes, selection rules imposed by energy and quasimomentum conservation in Eq. (2) imply a severely reduced three-phonon scattering phase space available to long-wavelength LA modes. In Fig. 2, we show total LA scattering rates under varying tensile strain amplitudes at different wavelength scales. Decomposing our data for small k , we detect three different types of scattering channels that contribute to the total LA rate in the long-wavelength limit: $\text{LA} \rightarrow \text{FA} + \text{FA}$, $\text{LA} \rightarrow \text{TW} + \text{TW}$, and $\text{LA} + \text{OPT} \rightarrow \text{OPT}$ among which the first dominates in both unstrained and strained tubes.

In the absence of lattice strain, one finds $\Gamma_{\text{LA}}^{\epsilon=0} \sim \Gamma_{\text{LFF}}^- \sim k^{-1/2}$ which can be traced back to the long-wavelength scaling relations $\omega_{\text{FA}} \sim k^2$ and $V_{\text{LFF}} \sim kk'k''$ (see Appendix B1). As can be noted from the top left-hand panel of Fig. 2, the square root scaling breaks down at smaller wavelength scales $ka > 0.1\pi$. This threshold conforms with the phonon dispersion data in Fig. 1,

where it can be seen that FA mode frequencies deviate from the quadratic trend once $ka > 0.1\pi$, indicating a regime where atomistic details entering into the exact phonon dispersion become important.

In the presence of tensile lattice strain, $\epsilon > 0$, lattice-dynamical predictions in Fig. 2 indicate a reduction of long-wavelength rates with increasing strain amplitude and a transition away from the square root scaling in unstrained tubes. In order to explain the strain dependence of Γ_{LA} , we resolve Γ_{LFF}^- as per Eqs. (1) and (2) in the continuum limit $\sum_k \rightarrow \int dk$ which requires knowledge of the functional wave number dependencies of ω_{LA} , ω_{FA} and V_{LFF} . Here, we adopt the dispersion fit lines of Fig. 1 and, under the assumption that strain has no effect on the cubic wave number dependence of three-phonon couplings, we set $V_{\text{LFF}} = C_3 kk'k''$. Representing the three-phonon coupling strength, the only unknown parameter C_3 is then fitted to lattice-dynamical data of Γ_{LFF}^- . This procedure yields the solid lines in Fig. 2 for tubes in unstrained and strained configurations. In fitting our lattice-dynamical predictions, we do not observe a systematic variation of C_3 under varying strain amplitudes, $C_3 \approx \epsilon$, which leaves ω_{FA} as the only strain dependent quantity entering into Γ_{LFF}^- . Thus, the strain induced downward shift of LA rates can be solely attributed to the frequency hardening of FA modes.

The implications of a linearized FA mode dispersion are best understood in the phonon frequency domain, where the density of FA states D_{FA} within the low-frequency interval $\omega + d\omega$ goes from $D_{\text{FA}} \sim \omega^{-1/2}$ in unstrained to $D_{\text{FA}} \sim \omega^0$ in strained systems. Loosely speaking, under increasing tensile lattice strain, there are less and less preferential FA states that a given long-wavelength LA mode can decay into. Assuming a strictly linear FA mode dispersion with strain dependent prefactor, $\omega_{\text{FA}} \sim \epsilon^{1/2}|k|$, one finds $\Gamma_{\text{LA}}^{\epsilon>0} \sim \Gamma_{\text{LFF}}^- \sim \epsilon^{-5/2}k^2$ (see Appendix B1).

The scattering amplitudes Γ_{LTT}^- and Γ_{LOO}^+ , both of which do not involve long-wavelength FA modes, remain relatively insensitive to strain. A scaling behavior $\Gamma_{\text{LTT}}^- \sim k^2$ is deducible from a linear dispersion $\omega_{\text{TW}} \sim |k|$ and a coupling coefficient $V_{\text{LTT}} \sim kk'k''$ (see Appendix B3). To produce the solid lines in Fig. 2 for Γ_{LTT}^- , as before, the unknown prefactor of V_{LTT} is taken as a fit parameter to our lattice-dynamical predictions. In the case of optical absorption processes, numerical noise inherent to our evaluation of Eqs. (1) and (2) becomes apparent to the extent that no continuous trend lines for Γ_{LOO}^+ are discernable. Notwithstanding the uncertainty in our prediction of Γ_{LOO}^+ , data points in Fig. 2 suggest that optical absorption processes as well as TW mode interactions contribute negligibly to the dissipation of long-wavelength LA modes.

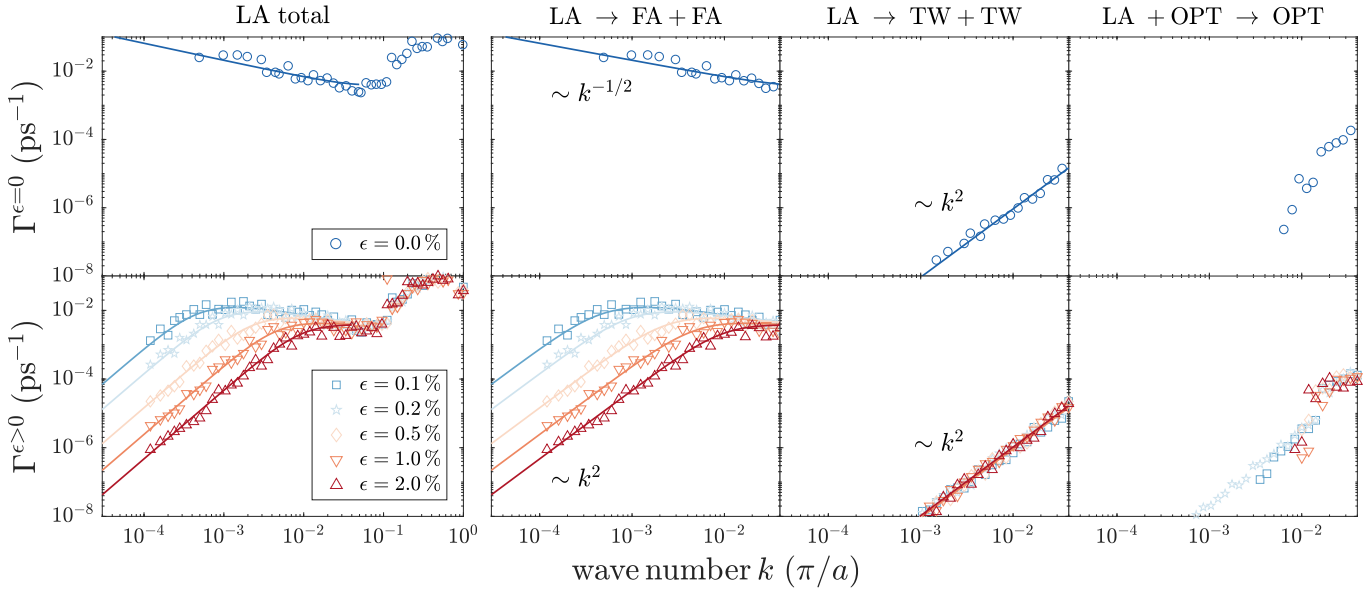


FIG. 2. Anharmonic scattering rates (left) of LA modes at room temperature and decomposition (right) into individual three-phonon scattering channels in the region $k \leq 0.04\pi/a$. Top and bottom panels show stress-free, $\epsilon = 0$, and stretched, $\epsilon > 0$, configurations of a (4,4) carbon nanotube, respectively. Lattice-dynamical predictions as per Eqs. (1) and (2) are represented by empty plot markers. Solid curves are obtained by substituting long-wavelength approximations into Eqs. (1) and (2). In the $ka \ll 1$ limit, the total LA scattering rate is dominated by the decay process LA \rightarrow FA + FA. Induced by strain, frequency hardening of FA modes causes total scattering rates to transition from a scaling $\sim k^{-1/2}$ in stress-free tubes to a scaling $\sim \epsilon^{-5/2}k^2$ in strained tubes.

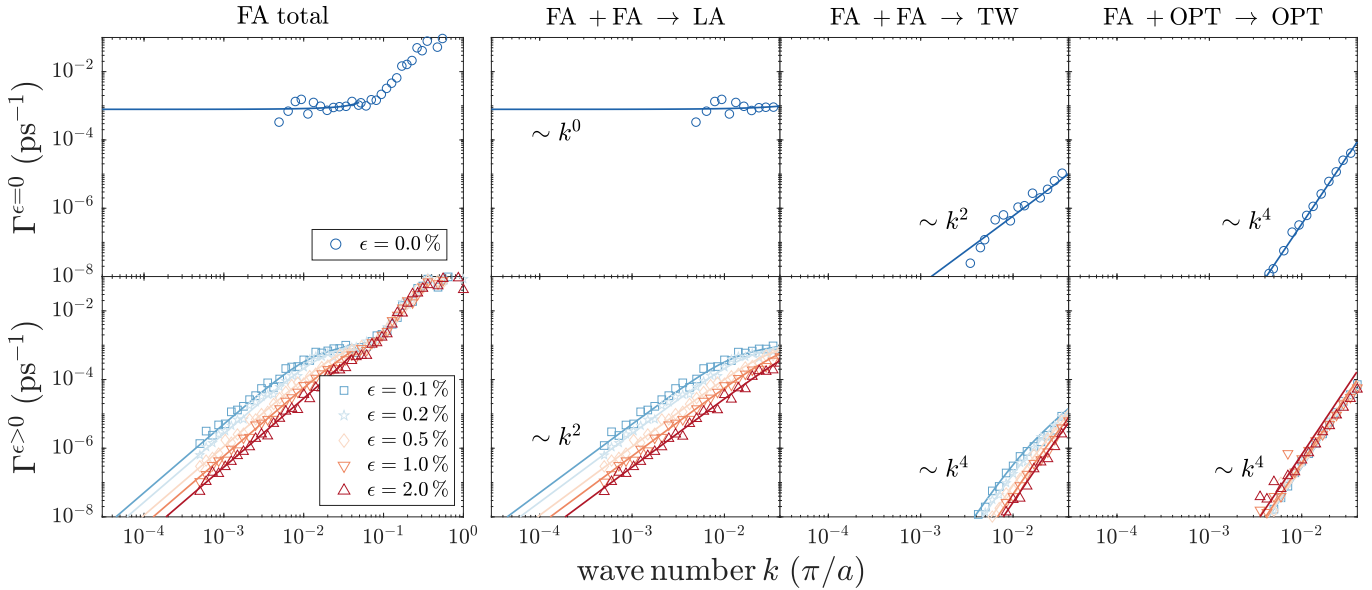


FIG. 3. Same as Fig. 2 but for FA modes. Both FA + FA \rightarrow LA and FA + FA \rightarrow TW absorption processes are affected by the strain induced frequency shift of FA modes in the limit $ka \ll 1$. As dictated by the dominant scattering channel FA + FA \rightarrow LA, total FA scattering rates converge towards a constant in the case of stress-free tubes and gain a dependence $\sim \epsilon^{-1}k^2$ in the presence of strain.

B. Flexural modes

Generally speaking, the three-phonon scattering phase space for long-wavelength FA modes is reduced in that no lower-lying phonon branch providing pathways for kin-

ematically allowed decay processes exists. Our lattice-dynamical predictions of strain dependent FA scattering rates are summarized in Fig. 3. In the limit $ka \ll 1$, traceable scattering contributions arise from two types of acoustic absorptions that depend critically on tensile

strain, namely $\text{FA} + \text{FA} \rightarrow \text{LA}$ as well as $\text{FA} + \text{FA} \rightarrow \text{TW}$, and from optical interbranch absorptions $\text{FA} + \text{OPT} \rightarrow \text{OPT}$ which appear unaffected by strain.

As is evident in Fig. 3, a reduction in the total scattering rate of long-wavelength FA modes under increasing tensile lattice strain derives from the dominant process $\text{FA} + \text{FA} \rightarrow \text{LA}$. The same three-phonon coupling coefficient V_{LFF} enters into decay Γ_{LFF}^- and absorption amplitudes Γ_{FFL}^+ . Hence, according to our earlier observation $V_{\text{LFF}} \approx \epsilon$ in the case of LA modes, a reduction in the total rate should be solely ascribable to the strain induced hardening of FA modes. Indeed, by setting $V_{\text{LFF}} = C_3 k k' k''$ and by fitting our lattice-dynamical predictions of Γ_{FFL}^+ for different tensile strain amplitudes ϵ , we find no systematic variation of C_3 with increasing tensile strain, leaving only ω_{FA} as a strain dependent factor. Based on analytical considerations of Γ_{FFL}^+ , adopting either a quadratic $\omega_{\text{FA}} \sim k^2$, or a strictly linear FA mode dispersion $\omega_{\text{FA}} \sim \epsilon^{1/2}|k|$, stress-free and stretched tubes give rise to $\Gamma_{\text{FA}}^{\epsilon=0} \sim k^0$ and $\Gamma_{\text{FA}}^{\epsilon>0} \sim \epsilon^{-1}k^2$, respectively (see Appendix B 2).

Comparing the absorption channels $\text{FA} + \text{FA} \rightarrow \text{LA}$ and $\text{FA} + \text{FA} \rightarrow \text{TW}$, the scaling relations of the latter $\Gamma_{\text{FFT}}^+ \sim k^2$ in unstrained and $\Gamma_{\text{FFT}}^+ \sim \epsilon^{-1}k^4$ in strained tubes stem from $V_{\text{TFF}} \sim k k' k'' (k' - k'')$ (see Appendix B 2). In our lattice-dynamical calculations of V_{TFF} , contributions that are cubic in the axial wave number k cancel out, in agreement with elasticity theory predictions [27]. Similar cancellation effects manifest in the case of optical absorption processes $\text{FA} + \text{OPT} \rightarrow \text{OPT}$. Following a standard argument [36], for a given long-wavelength acoustic phonon (j, k) , one expects a linear scaling $V_{j\text{OO}} \sim k$ to lowest order in k . In order to explain the scaling $\Gamma_{\text{FOO}}^+ \sim k^4$ of optical interbranch transitions in Fig. 3, however, we have to assume $V_{\text{FOO}} \sim k^2$ (see Appendix B 4).

C. Twisting modes

The branch of long-wavelength TW modes lies in the regime $\omega_{\text{FA}} < \omega_{\text{TW}} < \omega_{\text{LA}}$ and, as compared to LA and FA modes, a kinematically less restricted three-phonon scattering phase space may be anticipated. As shown in Fig. 4, three-phonon transitions that contribute to the dissipation of long-wavelength TW modes can be decomposed into two types of low-energy acoustic and two types of high-energy optical scattering channels. The former channels are $\text{TW} \rightarrow \text{FA} + \text{FA}$ and $\text{TW} + \text{TW} \rightarrow \text{LA}$, while the latter are given by intra- and interbranch absorptions, $\text{TW} + \text{OPT}_a \rightarrow \text{OPT}_a$ and $\text{TW} + \text{OPT}_a \rightarrow \text{OPT}_b$, respectively. The relative importance of these channels varies with tensile strain, causing a nontrivial strain dependence in the total rate Γ_{TW} .

In the case of unstrained tubes, $\epsilon = 0$, the dominant scattering amplitudes stem from the decay into two flexural modes, Γ_{TFF}^- , and from optical intrabranch absorptions, $\Gamma_{\text{TO}_a\text{O}_a}^+$, both of which are roughly of the same

order of magnitude within the resolved range of wave numbers. For the decay $\text{TW} \rightarrow \text{FA} + \text{FA}$, we have $\Gamma_{\text{TFF}}^- \sim k^{1/2}$ which is derivable given a quartic scaling of V_{TFF} and provided that $\omega_{\text{FA}} \sim k^2$ under stress-free conditions (see Appendix B 1). Considering optical absorption processes of acoustic modes, the scaling behavior of related scattering amplitudes depends on whether momentum is transferred between two crossing optical branches or within the same branch. If we adopt the long-wavelength approximation $V_{\text{TOO}} \sim k$ [36], we find that differences in the scattering phase space lead to $\Gamma_{\text{TO}_a\text{O}_a}^+ \sim k$ and $\Gamma_{\text{TO}_a\text{O}_b}^+ \sim k^2$, explaining the scaling of intra- and interbranch transitions in Fig. 4, respectively (see Appendix B 4).

In the presence of tensile strain, $\epsilon > 0$, as before in the case of Γ_{LFF}^- , Γ_{FFL}^+ , and Γ_{FFT}^+ , frequency hardening of long-wavelength FA modes strongly suppresses the scattering amplitude of $\text{TW} \rightarrow \text{FA} + \text{FA}$ decay. Applying a fit to our lattice-dynamical predictions of Γ_{TFF}^- , we again notice that strain has no influence on the coupling coefficient V_{TFF} , whose quartic wave number dependence together with $\omega_{\text{FA}} \sim \epsilon^{1/2}|k|$ yields $\Gamma_{\text{TFF}}^- \sim \epsilon^{-7/2}k^4$ (see Appendix B 1). For moderately strained tubes, total TW scattering rates in the long-wavelength limit remain lower bounded by optical intrabranch transitions and the limiting behavior transitions from $\sim k^{1/2}$ to $\sim k$.

Interestingly, at larger strain amplitudes, long-wavelength scattering contributions arising from optical intrabranch absorption processes may become susceptible to lattice strain as well. For our model of a (4,4) carbon nanotube, we find that optical intrabranch transitions can occur only in the regime $\epsilon < 4\%$ beyond which the total TW rate abruptly gains a k^2 dependence resulting from optical interbranch transitions. While no structural changes can be observed in the carbon lattice at $\epsilon = 4\%$, an explanation for the discontinuity in the total TW rate is found by considering the strain dependence of optical phonon frequencies, see Fig. 5. A necessary condition for the realization of intrabranch transitions is the existence of a supersonic optical branch ω_{OPT^*} . As illustrated in Fig. 5(a), one such branch whose slope $\partial\omega_{\text{OPT}^*}/\partial k$ surpasses the slope of the TW branch can be singled out in the spectrum of high-energy optical modes. Under tensile loading, the branch ω_{OPT^*} softens, cf. Fig. 5(b), and its slope decreases. Figure 5(c) demonstrates that for strain amplitudes $\epsilon \geq 4\%$ the necessary condition $\partial\omega_{\text{OPT}^*}/\partial k > v_{\text{TW}}$ for optical intrabranch transitions is no longer fulfilled. A somewhat pathological prediction of Eq. (2) reveals itself as the critical strain amplitude $\epsilon = 4\%$ is approached from below. Here, scattering rates are predicted to increase, which can be traced to the vanishing curvature, $\partial^2\omega_{\text{OPT}^*}/\partial k^2 \rightarrow 0$, in the wave number regions depicted by the insets of Fig. 5(a), cf. Eqs. (B2) and (B14). In passing, we can compare TW and LA mode velocities in Fig. 5(c) to conclude that long-wavelength LA modes remain protected from optical intrabranch transitions.

We point out that a recent numerical study on un-

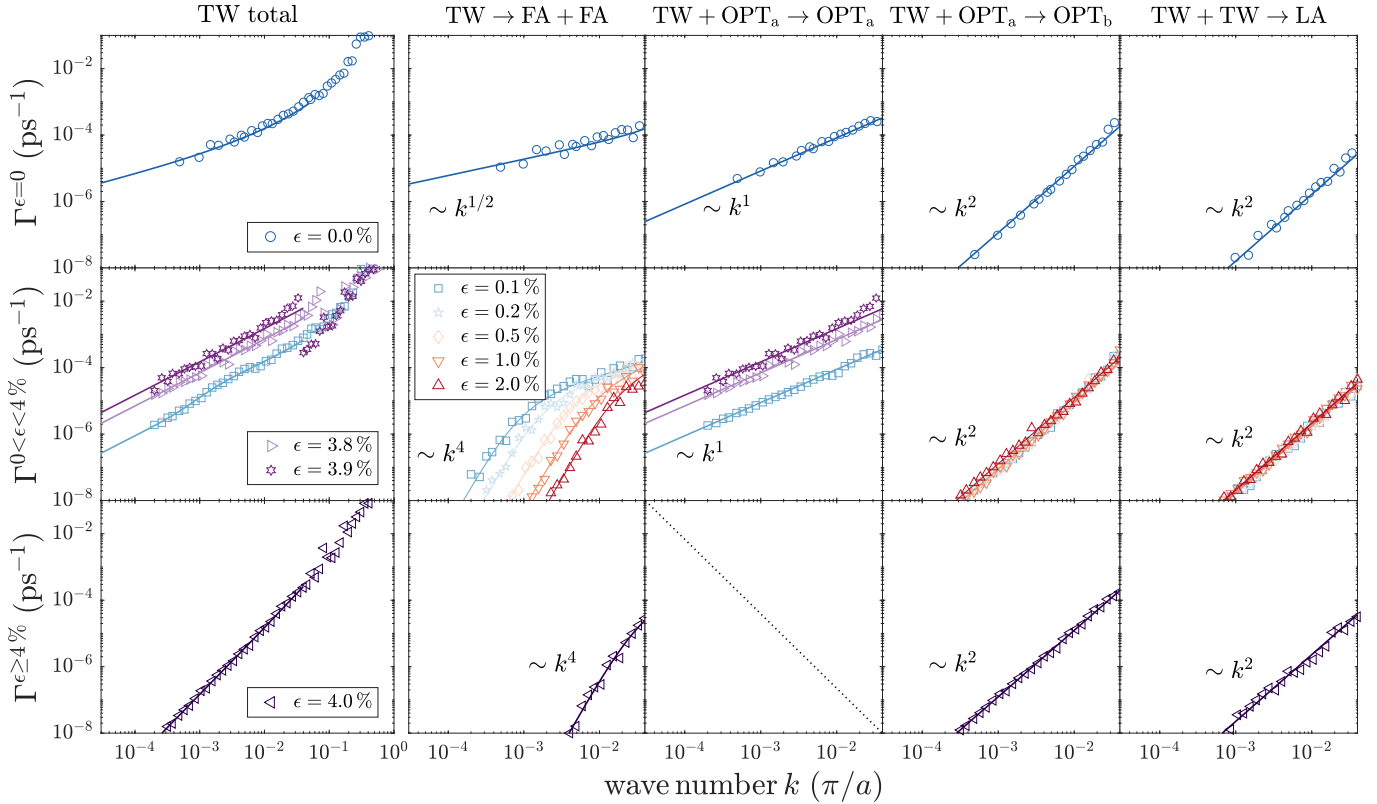


FIG. 4. Same as Fig. 2 but for TW modes. A third row of panels is added to distinguish the strain regimes $0 < \epsilon < 4\%$ (middle) and $\epsilon \geq 4\%$ (bottom). Processes involving two optical modes are further subdivided into contributions resulting from intrabranch, $\text{TW} + \text{OPT}_a \rightarrow \text{OPT}_a$ and interbranch, $\text{TW} + \text{OPT}_a \rightarrow \text{OPT}_b$, transitions whose long-wavelength scaling is $\sim k$ and $\sim k^2$, respectively. For stress-free tubes, the decay process $\text{TW} \rightarrow \text{FA} + \text{FA}$ goes as $\sim k^{1/2}$ and becomes the dominant contribution to the total rate in the limit $ka \ll 1$. Under finite positive strain, $\epsilon > 0$, this process develops a dependence $\sim \epsilon^{-7/2}k^4$ such that the scaling of the total becomes $\sim k$ due to optical intrabranch transitions, which are kinematically allowed as long as $\epsilon < 4\%$. In the strain regime $\epsilon \geq 4\%$, the total TW scattering rate inherits a dependence $\sim k^2$ stemming from optical interbranch transitions.

strained nanowires by Rashid et al. [37] found low-frequency power-law dependencies of three-phonon scattering rates for LA, FA, and TW modes that conform to our results for unstrained tubes. From the viewpoint of acoustic phonons, nanowires and nanotubes are very similar. It seems therefore natural to conjecture that considerations in the present study apply to a broader class of one-dimensional materials, implying, for example, that a strain induced reduction in the scattering strength of long-wavelength acoustic phonons can be achieved in nanowires as well.

V. THERMAL CONDUCTIVITY UNDER THE RELAXATION TIME APPROXIMATION

Three-phonon scattering rates presented in Figs. 2-4 are a key ingredient for determining the lattice thermal conductivity of pristine nanotubes in the framework of the PBE. Under the single-mode relaxation time approximation (RTA)[38], the thermal conductivity of carbon

nanotubes is given by

$$\kappa^{\text{RTA}} = \frac{1}{A} \sum_j \int_{-\pi/a}^{\pi/a} \frac{dk}{2\pi} \hbar \omega_\nu \frac{\partial n_\nu}{\partial T} v_\nu^2 \tau_\nu, \quad (5)$$

where typically an annular cross-sectional area $A = \pi D \delta$ is adopted with thickness $\delta = 3.35 \text{ \AA}$ corresponding to the interlayer distance in graphite, the phonon velocity is taken as the slope of dispersion branches, $v_\nu = \partial \omega_\nu / \partial k$, and τ_ν denotes the phonon relaxation time. Following the standard practice within the PBE formalism, intrinsic three-phonon scattering rates as per Eqs. (1) and (2) are combined with a boundary scattering rate to compute phonon relaxation times in tubes of finite length L ,

$$\frac{1}{\tau_\nu} = \Gamma_\nu + \frac{2|v_\nu|}{L}. \quad (6)$$

The boundary scattering term acts as an upper bound to phonon relaxation times, which effectively filters out contributions from low-frequency modes with small intrinsic scattering rates and ensures a ballistic transport regime

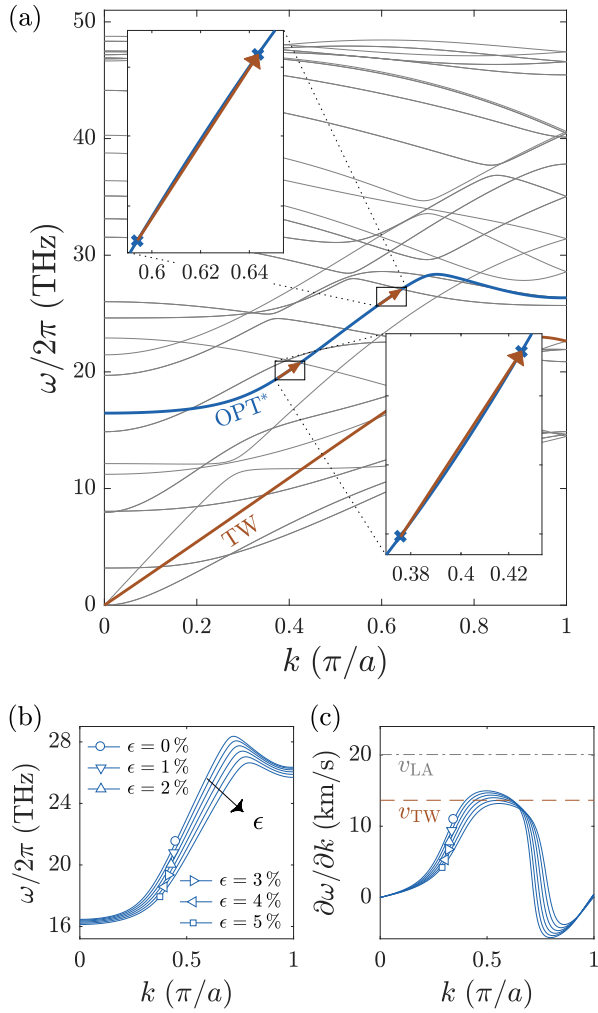


FIG. 5. (a) The spectrum of harmonic phonon modes of a (4,4) carbon nanotube at $\epsilon = 0$ comprises one optical branch (OPT*) whose slope matches the slope of the TW branch, enabling intrabrand transitions $\text{TW} + \text{OPT}_a \rightarrow \text{OPT}_a$. (b) Frequency softening of the OPT* branch under tensile strain. (c) The slope of the OPT* branch decreases with increasing strain amplitude. At $\epsilon = 4\%$, the velocity v_{TW} exceeds $\partial\omega_{\text{OPT}^*}/\partial k$ and the scattering of long-wavelength TW modes due to intrabrand transitions is kinematically prohibited.

$\kappa \sim L$ in the limit of short tubes [19]. Given the scaling laws of anharmonic phonon scattering $\Gamma_j(k) \sim \epsilon^r k^s$ found in Sec. IV, the integration over acoustic branch contributions in Eq. (5) converges for $L \rightarrow \infty$ in stress-free tubes, $\epsilon = 0$, but diverges in the presence of strain, $\epsilon > 0$ (see Appendix C).

Usually, per-mode conductivities as per Eq. (5) are sampled and summed over a finite grid of wave numbers, $\kappa^\Sigma = N^{-1} \sum_j \sum_k \kappa_j(k)$, with grid spacing $\Delta k = 2\pi/Na$, which requires to test convergence with respect to N . Such an approach, however, is problematic if intrinsic lifetimes exhibit a divergence, $(\Gamma_\nu)^{-1} \rightarrow \infty$ for $|k| \rightarrow 0$, as is the case for LA and FA modes in strained and for TW modes in both unstrained and strained tubes. For

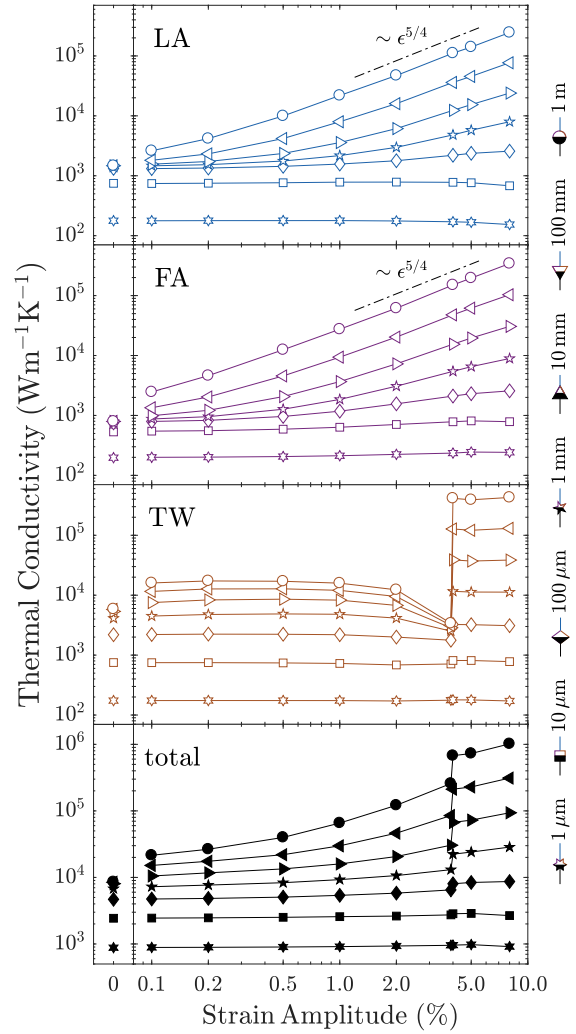


FIG. 6. Lattice thermal conductivity under the relaxation time approximation of a pristine (4,4) carbon nanotube at room temperature as derived from strain-dependent three-phonon scattering rates. In stress-free tubes, $\epsilon = 0$, the conductivity converges with tube length L . Under finite tensile strain, $\epsilon > 0$, and in the limit of long tubes, the acoustic phonon contributions to the lattice thermal conductivity scale as $\kappa_{\text{LA/FA}} \sim \epsilon^{5/4} L^{1/2}$ and as $\kappa_{\text{TW}} \sim \ln L$ ($\sim L^{1/2}$) for $\epsilon < 4\%$ ($\geq 4\%$).

large but finite values of L , sufficiently dense wave number grids to converge the thermal conductivity might be out of reach by means of lattice-dynamical calculations. Here, for our model of a (4,4) carbon nanotube, we use the asymptotic fits to dispersion laws and three-phonon scattering rates as depicted in Figs. 1-4 in order to extrapolate the wave number dependencies of acoustic per-branch conductivities in the $|k| \rightarrow 0$ limit. This in turn allows us to numerically integrate acoustic long-wavelength contributions all the way down to the Gamma point ($k = 0$), $\kappa^{\text{LW}} = \int_0 dk \kappa_j(k)$ for $j \in \{\text{LA, FA, TW}\}$.

In Fig. 6, we combine per-mode conductivities sampled over a grid with $N = 1000$ points with acoustic mode con-

tributions integrated over the interval $[-2\pi/Na; 2\pi/Na]$, $\kappa = \kappa^\Sigma + \kappa^{\text{LW}}$, to show the conductivity predictions according to Eqs. (5) and (6) in the limit of small strain amplitudes ϵ . The relative importance of summed κ^Σ vs integrated long-wavelength contributions κ^{LW} is displayed in Fig. 7. As can be seen in Fig. 6, relatively long tubes $L > 100 \mu\text{m}$ are required to observe an enhancement of thermal transport due to a reduction in the scattering rates of long-wavelength acoustic modes in the presence of strain. For a tube with fixed but very large L , frequency resolved conductivity contributions shift towards lower frequencies with increasing strain amplitude. The lowest contributing frequencies, however, are ultimately determined by the tube length since, in principle, low-frequency acoustic modes of wave number k cannot exist in tubes of size L unless $1/k < L$.

In the long-tube limit, LA modes in strained tubes yield a conductivity contribution that scales as $\sim \epsilon^{5/4} L^{1/2}$ which follows from $\Gamma_{\text{LA}} \sim \epsilon^{5/2} k^2$. The same scaling relation is obtained in the case of FA branch contributions which, in this case, is attributable to $\Gamma_{\text{FA}} \sim \epsilon^{-1} k^2$ as well as $\omega_{\text{FA}} \sim \epsilon^{1/2} k$. For TW modes, the long-wavelength scaling relation $\Gamma_{\text{TW}} \sim k$ leads to a logarithmically divergent conductivity contribution in tubes subject to strain amplitudes $0 < \epsilon < 4\%$. The discontinuity in the strain dependence of long-wavelength TW scattering rates at $\epsilon = 4\%$, as detailed in Fig. 5, is filtered out in short tubes but becomes apparent if $L > 10 \mu\text{m}$. For strain amplitudes $\epsilon \geq 4\%$, a divergence $\sim L^{1/2}$ of the TW branch conductivity contribution is implied by $\Gamma_{\text{TW}} \sim k^2$. In the bottom panel of Fig. 6, we show total thermal conductivity predictions including optical branch contributions which, however, do not increase significantly with tube length, and are therefore of minor importance in the large- L regime. Remarkably, under the RTA, long-wavelength TW modes are predicted to be the dominant heat carriers in unstrained tubes as the tube length approaches the millimeter length scale.

As can be inferred from Fig. 7, per-branch acoustic conductivity data sampled over a grid with $N = 1000$ discrete wave numbers gives a poor representation of the total thermal conductivity according to Eqs. (5) and (6) as the tube length L becomes large. In unstrained tubes, $\epsilon = 0$, it is the square root divergence of intrinsic TW lifetimes $(\Gamma_{\text{TW}})^{-1} \sim k^{-1/2}$ which requires grid calculations with $N \gg 1000$ to converge conductivity predictions in the long-tube limit. Convergence issues with respect to the wave number grid resolution N are generally exacerbated in the presence of tensile strain, $\epsilon > 0$, where all three acoustic mode polarizations exhibit a singularity of the form $(\Gamma_j)^{-1} \sim k^{-r}$ with $r \geq 1$ in the long-wavelength limit.

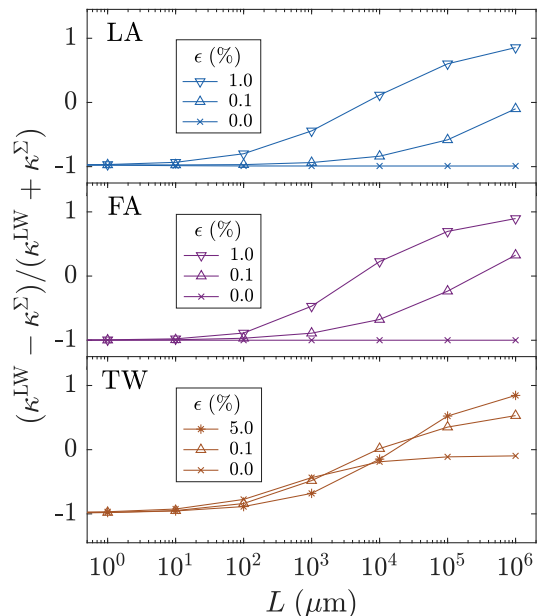


FIG. 7. Relative importance of summed κ^Σ vs integrated κ^{LW} acoustic thermal conductivity contributions as a function of tube length L and strain amplitude ϵ . κ^Σ corresponds to a summation over a wave number grid with $N = 1000$ points. Extrapolated contributions stemming from long-wavelength acoustic modes in close proximity to the Gamma point ($k = 0$) are captured by κ^{LW} but not included in κ^Σ . A value of -1 on the vertical axis implies a convergence of thermal conductivity with respect to the wave number grid resolution N , whereas larger values justify an extrapolation approach.

VI. DISCUSSION

Two approximations have been employed in the present study that deserve further scrutiny in the future. For one, phonon frequency shifts at finite temperature induced by lattice anharmonicity have been assumed to be negligible. In the case of two-dimensional crystals, by taking into account the real part of the phonon self-energy, it was noted [39] that out-of-plane vibrations are renormalized at finite temperature to the extent that the quadratic dispersion in stress-free samples under the harmonic lattice approximation becomes linear in the long-wavelength limit. For unstrained tubes, the obtained scaling laws of three-phonon scattering presented in Sec. IV critically depend on the condition that FA mode frequencies vanish quadratically in the long-wavelength limit, $\omega_{\text{FA}} \sim k^2$. Taking a temperature dependent, possibly linearized, FA mode dispersion as input to a perturbative calculation of phonon-phonon interactions, low-frequency dissipation rates $\Gamma_j(|k| \rightarrow 0)$ could be drastically decreased, as we demonstrate in this work by examining tubes under tensile load. In a similar context, while studying phonon-phonon interactions in a semiflexible monoatomic chain, Santhosh and Kumar [40] pointed out the necessity of anharmonic frequency renormalization, since the standard perturbative treatment of harmonic phonon modes vio-

lates the notion of well-defined quasiparticles, requiring $\Gamma_j(k) < \omega_j(k)$ as $|k| \rightarrow 0$. In particular, according to Ref. [40], longitudinal, $\omega_x \sim k$, and transverse, $\omega_y \sim k^2$, modes of a semiflexible chain under the harmonic lattice approximation give rise to $\Gamma_x \sim |k|^{-1/2}$ and $\Gamma_y \sim k^0$, in agreement with our findings for LA and FA modes in unstrained tubes, cf. Sec. IV A and Sec. IV B. Effective long-wavelength dissipation rates under phonon renormalization, as predicted in Ref. [40], are instead significantly reduced.

Another point worthy of future research relates to the approximation of thermal conductivity. Previous studies emphasized the inadequacy of the RTA in the case of one- [21, 24, 41, 42] and two-dimensional [17, 18, 43, 44] materials, noting the importance of obtaining the thermal conductivity from an exact solution of the PBE. Going beyond the RTA, one is confronted with numerically solving a large set of linear equations [38, 45],

$$X_\nu = \sum_{\nu'} P_{\nu\nu'} \psi_{\nu'}. \quad (7)$$

Here, the inhomogeneity X_ν and the collision kernel $P_{\nu\nu'}$ are given in terms of phonon dispersion data and phonon scattering rates, respectively, while the unknowns ψ_ν are the nonequilibrium phonon deviation functions, which ultimately determine the thermal conductivity, $\kappa \sim N^{-1} \sum_\nu X_\nu \psi_\nu$ (up to some prefactors) [38, 45]. The RTA approach to lattice heat transport, as pursued in Sec. V, is tantamount to keeping only the diagonal terms of the collision kernel, $(P\psi)_\nu \approx P_\nu \psi_\nu$ [38, 45]. It is sometimes noted that RTA predictions generally underestimate the true thermal conductivity [46, 47]. Therefore, given our results presented in Sec. V, one is tempted to conclude that nanotubes under tensile strain act as superdiffusive heat conductors which give rise to $\kappa \sim L^\eta$ with $\eta \geq 1/2$ in the long-tube limit. In the case of graphene, a similar reasoning based on the RTA was applied by the authors of Ref. [16] to conclude that the thermal conductivity of isotropically strained sheets should be logarithmically divergent with domain size. In pursuing an exact solution approach, however, some of the same authors later arrived at the conclusion that the conductivity of pristine graphene should remain upper bounded, even in the presence of strain [17]. By taking into account the low-frequency three-phonon scattering rates of Sec. IV, it would be desirable to make more rigorous analytical statements about the long-tube limit of thermal conductivity based on Eq. (7). Very recently, a convergence with tube length was reported by Barbalinardo et al. [24], who derived the thermal conductivity of a (10,0) nanotube in stress-free condition by numerically inverting the full collision kernel $P_{\nu\nu'}$. Under the assumption of tubes in perfect mechanical equilibrium, such convergent behavior falls into line with RTA level predictions. Still, the role of tensile strain within exact solution approaches to the PBE remains to be clarified.

VII. CONCLUSIONS

Taking as example a (4,4) carbon nanotube, we have performed numerical lattice-dynamical calculations to address the role of acoustic phonons in low-dimensional nanotube heat transport. By supporting our calculations with analytical considerations and by making recourse to continuum theories, we derived the general long-wavelength scaling relations of acoustic phonon scattering rates that follow from standard anharmonic perturbation theory. Based on our model, the onset of long-wavelength behavior in tubes of radius R is predicted at around $|k|R < 0.3$. We expect that somewhat smaller wave numbers are needed in the case of chiral nanotubes, which tend to have larger translational unit cells.

As was shown earlier in the case of graphene [16], the three-phonon scattering strength of long-wavelength acoustic modes can be reduced by tensile lattice strain whenever acoustic-flexural mode type processes are dominant. The scattering phase space for these processes is greatly reduced by a strain-induced hardening of flexural mode frequencies. In going from a two-dimensional phonon scattering phase space in graphene to a one-dimensional one, this effect becomes even more pronounced in nanotubes. As compared to longitudinal modes, long-wavelength twisting modes in nanotubes couple only weakly to flexural modes. Twisting modes have divergent anharmonic lifetimes in the long-wavelength limit in both unstrained and strained tube configurations, which makes k -space integration in the PBE-RTA formalism challenging.

Arguably, for nanotubes under tensile strain, PBE-RTA predictions provide strong evidence for the nonexistence of an upper bound to thermal conductivity, suggesting the possibility of superdiffusive heat transport in macroscopically long nanotubes. Whether exact solution approaches to the PBE, or the systematic inclusion of four-phonon scattering processes, help to renormalize a formally divergent thermal conductivity awaits further investigation.

ACKNOWLEDGMENTS

The authors gratefully acknowledge financial support from the Discovery Grant Program of the Natural Sciences and Engineering Research Council of Canada. D.B. was supported by the QuEST fellowship at the University of British Columbia. This research was undertaken thanks, in part, to funding from the Canada First Research Excellence Fund, Quantum Materials and Future Technologies Program.

Appendix A: Three-phonon coupling coefficients

For a one-dimensional monoatomic crystal, the three-phonon coupling coefficients entering into Eq. (2) are given by [35, 48]

$$V_{jj'j''}(k, k', k'') = \frac{1}{m^{3/2}} \sum_{L', L''} e^{ik'r_{L'}} e^{ik''r_{L''}} \sum_{l, l', l''} \sum_{\alpha, \alpha', \alpha''} w_l^\alpha(j, k) w_{l'}^{\alpha'}(j', k') w_{l''}^{\alpha''}(j'', k'') \Phi_{0l, L', L'', l''}^{\alpha, \alpha', \alpha''}, \quad (\text{A1})$$

where m denotes the atomic mass, the first sum runs over translational unit cells residing at $r_{L'}$ ($r_{L''}$), the second sum runs over atomic sites within a unit cell, the third sum extends over Cartesian coordinates, the w 's are the harmonic phonon eigenvectors, and Φ is the third order force constant tensor.

For carbon nanotubes, in order to accurately determine the coupling coefficients of acoustic phonons in the limit of small wave numbers, it is crucial to ensure that the tensor Φ obeys translational and rotational sum rules [25]. By adopting an empirical Tersoff type interaction potential and by deriving force constants analytically, these sum rules are naturally captured in our calculations.

Appendix B: Three-phonon scattering rates in the low-frequency limit

Starting from Eqs. (1) and (2), we aim to determine the scaling of the transition amplitudes $\Gamma_{jj'j''}^\pm(k)$ for acoustic modes, $j \in \{\text{LA, FA, TW}\}$, in the long-wavelength limit $0 < ka \ll 1$. The quasimomentum selection rule $\Delta_{k \pm k' - k'', 2\pi m/a}$ in Eq. (2) can be invoked to resolve the sum over k'' in Eq. (1). Setting $k'' = k \pm k' - 2\pi m/a$, the integer $m = 0, \pm 1$ is chosen such that the sum $k \pm k'$ lies within the first zone $[-\pi/a; \pi/a]$. Three-phonon scattering events involving low-frequency phonons necessarily correspond to normal processes ($m = 0$) [49], and for a given mode triplet (j, j', j'') we have

$$\Gamma_{jj'j''}^\pm(k) = \frac{a}{2\pi} \int_{-\pi/a}^{\pi/a} dk' \frac{\hbar\pi}{4\omega_j(k)\omega_{j'}(k')\omega_{j''}(k \pm k')} \frac{[n_{j'}(k') + \frac{1}{2} \pm \frac{1}{2}] n_{j''}(k \pm k')}{n_j(k)} \times |V_{jj'j''}(k, \pm k', -k \mp k')|^2 \delta(\Omega_{jj'j''}^\pm(k, k')), \quad (\text{B1})$$

where the function $\Omega_{jj'j''}^\pm(k, k') = \omega_j(k) \pm \omega_{j'}(k') - \omega_{j''}(k \pm k')$ is introduced to represent the condition of energy conservation. Noting that $n_j(k) = [\exp(\hbar\omega_j(k)/k_B T) - 1]^{-1} \approx k_B T / \hbar\omega_j(k)$, Eq. (B1) becomes

$$\Gamma_{jj'j''}^\pm(k) \sim \frac{[n_{j'}(k^*) + \frac{1}{2} \pm \frac{1}{2}] n_{j''}(k \pm k^*) |V_{jj'j''}(k, \pm k^*, -k \mp k^*)|^2}{\omega_{j'}(k^*) \omega_{j''}(k \pm k^*) \left| \frac{\partial \Omega_{jj'j''}^\pm(k, k^*)}{\partial k'} \right|}, \quad (\text{B2})$$

where the wave number $k^* = k_{jj'j''}^*(k)$ follows from $\Omega_{jj'j''}^\pm(k, k^*) = 0$.

1. Decay into two flexural modes

Let us first consider transitions where a long-wavelength acoustic phonon from a linear branch decays into two flexural acoustic modes, LA/TW \rightarrow FA + FA. As per Eqs. (3) and (4), k^* is the positive root of

$$\Omega^-(k, k^*) = v_j k - \sqrt{\mathcal{T}_1 \epsilon k^{*2} + \mathcal{Y}(\epsilon) k^{*4}} - \sqrt{\mathcal{T}_1 \epsilon (k - k^*)^2 + \mathcal{Y}(\epsilon) (k - k^*)^4} = 0, \quad (\text{B3})$$

where $v_j = v_{\text{LA/TW}}$ and $\mathcal{Y}(\epsilon) = v_{\text{LA}}^2 R^2 / 2 - \mathcal{T}_2 \epsilon$. The condition of energy conservation can be resolved analytically in two limiting cases by either assuming a strictly quadratic dispersion of flexural modes under stress-free conditions, $\omega_{\text{FA}} \sim k^2$, or by adopting a strictly linear dispersion in the presence of tensile strain ϵ , $\omega_{\text{FA}} \sim \epsilon^{1/2} k$. In the former scenario, we have

$$k^* = \frac{k}{2} + \sqrt{\frac{v_j}{2\mathcal{Y}(0)} k - \frac{k^2}{4}} \quad \text{and} \quad \left| \frac{\partial \Omega^-(k, k^*)}{\partial k'} \right| = 2\sqrt{2\sqrt{\mathcal{Y}(0)} v_j k - \mathcal{Y}(0) k^2}, \quad (\text{B4})$$

where both expressions go as $k^{1/2}$. In the low-frequency regime, $n_{\text{FA}}(k) \approx k_{\text{B}}T/\hbar\omega_{\text{FA}}(k)$, and by combining Eqs. (B2) and (B4) we find

$$\Gamma_{j\text{FF}}^-(k) \sim k^{-9/2} |V_{j\text{FF}}|^2 \sim \begin{cases} k^{-1/2} & \text{if } j = \text{LA}, \\ k^{1/2} & \text{if } j = \text{TW}, \end{cases} \quad (\text{B5})$$

where the standard long-wavelength approximation [35, 36] $V_{\text{LFF}} \sim kk'k''$ applies to $\text{LA} \rightarrow \text{FA} + \text{FA}$ but cancellation effects in Eq. (A1) lead to $V_{\text{TFF}} \sim kk'k''(k' - k'')$ [27] in the case of $\text{TW} \rightarrow \text{FA} + \text{FA}$.

If, on the other hand, a strictly linear flexural mode dispersion is assumed, $\omega_{\text{FA}} \sim \epsilon^{1/2}k$, we have

$$k^* = \left(1 + \frac{v_j}{\sqrt{\mathcal{T}_1\epsilon}}\right) \frac{k}{2} \quad \text{and} \quad \left| \frac{\partial\Omega^-(k, k^*)}{\partial k'} \right| = 2\sqrt{\mathcal{T}_1\epsilon}, \quad (\text{B6})$$

which, when plugged into Eq. (B2), leads to

$$\Gamma_{j\text{FF}}^-(k) \sim \epsilon^{-5/2} k^{-4} \frac{|V_{j\text{FF}}|^2}{(1 - v_j^2/\mathcal{T}_1\epsilon)^2} \sim \begin{cases} \epsilon^{-5/2} k^2 & \text{if } j = \text{LA}, \\ \epsilon^{-7/2} k^4 & \text{if } j = \text{TW}, \end{cases} \quad (\text{B7})$$

where the long-wavelength approximations of V_{LAFABA} and V_{TWAFABA} remain unaffected by tensile lattice strain, as suggested by our numerical evaluation of Eq. (A1).

2. Coalescence of two flexural modes

To determine the scaling of $\Gamma_{\text{FAFA}j''}^+$ for $j'' \in \{\text{LA}, \text{TW}\}$, we again solve the condition of energy conservation $\Omega^+(k, k^*) = 0$ for k^* and consider the cases $\omega_{\text{FA}} \sim k^2$ and $\omega_{\text{FA}} \sim \epsilon^{1/2}k^2$ separately. In the unstrained case, $\epsilon = 0$, we have

$$k^* = \frac{v_{j''}}{2\sqrt{\mathcal{Y}(0)}} - \sqrt{\frac{v_{j''}^2}{4\mathcal{Y}(0)} + \frac{v_{j''}}{\sqrt{\mathcal{Y}(0)}}k - k^2} \quad \text{and} \quad \left| \frac{\partial\Omega^+(k, k^*)}{\partial k'} \right| = \sqrt{v_{j''}^2 + 4\sqrt{\mathcal{Y}(0)}v_{j''}k - 4\mathcal{Y}(0)k^2}. \quad (\text{B8})$$

Here, the first expression goes as k and the second converges towards $v_{j''}$. In evaluating Eq. (B2), we can assume $n_{\text{FA}}(k) + 1 \approx k_{\text{B}}T/\hbar\omega_{\text{FA}}(k)$ and find

$$\Gamma_{\text{FF}j''}^+(k) \sim k^{-6} |V_{j''\text{FF}}|^2 \sim \begin{cases} k^0 & \text{if } j'' = \text{LA}, \\ k^2 & \text{if } j'' = \text{TW}, \end{cases} \quad (\text{B9})$$

where it is possible to reapply the long-wavelength approximations of V_{LFF} and V_{TFF} since $V_{jj'j''}(k, \pm k', -k \mp k')$ is symmetric under exchange of phonon indices $(j, k) \leftrightarrow (j, \pm k') \leftrightarrow (j'', -k \mp k')$ [48].

For strained tubes, $\epsilon > 0$, we find

$$k^* = \frac{\sqrt{\mathcal{T}_1\epsilon} - v_{j''}}{\sqrt{\mathcal{T}_1\epsilon} + v_{j''}} k \quad \text{and} \quad \left| \frac{\partial\Omega^+(k, k^*)}{\partial k'} \right| = \sqrt{\mathcal{T}_1\epsilon} + v_{j''} \quad (\text{B10})$$

and transition rates according to Eq. (B2) scale as

$$\Gamma_{\text{FF}j''}^+(k) \sim \epsilon^{-2} k^{-4} |V_{j''\text{FF}}|^2 \sim \begin{cases} \epsilon^{-1} k^2 & \text{if } j'' = \text{LA}, \\ \epsilon^{-1} k^4 & \text{if } j'' = \text{TW}. \end{cases} \quad (\text{B11})$$

3. One longitudinal and two twisting modes

In a similar manner, the strain independent scaling relations

$$\Gamma_{\text{LTT}}^-(k) \sim k^2 \quad \text{and} \quad \Gamma_{\text{TTL}}^+(k) \sim k^2 \quad (\text{B12})$$

can be inferred from Eq. (B2) by noting that $V_{\text{LTT}} \sim kk'k''$.

4. Absorption by optical phonons

If a low-energy acoustic mode (j, k) is absorbed by two high-energy optical phonons, energy conservation implies

$$\Omega^+(k, k^*) = \omega_j(k) + \omega_{\text{OPT}_a}(k^*) - \omega_{\text{OPT}_b}(k^* + k) = 0. \quad (\text{B13})$$

Such transitions manifest at some finite wave number $k^* \sim \text{const.}$ either in the form of intra-, $a = b$, or interbranch transitions, $a \neq b$, where two optical branches cross. For $ka \ll 1$, we can expand ω_{OPT_b} around k^* to show that

$$\left| \frac{\partial \Omega^+(k, k^*)}{\partial k'} \right| = \left| \frac{\partial \omega_{\text{OPT}_a}(k^*)}{\partial k'} - \frac{\partial \omega_{\text{OPT}_b}(k^*)}{\partial k'} - \frac{\partial^2 \omega_{\text{OPT}_b}(k^*)}{\partial k'^2} k - \dots \right| \sim \begin{cases} k & \text{if } a = b, \\ \text{const.} & \text{if } a \neq b, \end{cases} \quad (\text{B14})$$

and it follows from Eq. (B2) that transition rates scale as

$$\Gamma_{j\text{O}_a\text{O}_b}^+(k) \sim \begin{cases} k^{-1} |V_{j\text{OO}}|^2 & \text{if } a = b, \\ |V_{j\text{OO}}|^2 & \text{if } a \neq b. \end{cases} \quad (\text{B15})$$

Three-phonon coupling coefficients for one long-wavelength acoustic (j, k) and two optical phonons $V_{j\text{OO}}$ are of at least linear order in k [36]. Our data in Fig. 3 for optical interbranch transitions of FA modes suggests $V_{\text{FOO}} \sim k^2$, whereas the scaling behavior of TW modes as shown in Fig. 4 suggests $V_{\text{TFOO}} \sim k$ for both intra- and interbranch transitions.

Appendix C: Asymptotic strain and tube-length dependence of κ^{RTA}

Under the RTA, the conductivity contribution κ_j of long-wavelength acoustic modes in tubes of length L follows from Eqs. (5) and (6) as

$$\kappa_j \sim L \int_0^{k_{\text{cut}}} dk \frac{\xi_1^2 k^{2t}}{\xi_2 L k^s + \xi_1 k^t}, \quad (\text{C1})$$

where it is assumed that $n = k_{\text{B}}T/\hbar\omega$, $v = \xi_1 k^t$, and $\Gamma = \xi_2 k^s$ hold true below some finite wave number k_{cut} . For linear and quadratic dispersion branches, we have $t = 0$ and $t = 1$, respectively. The expression (C1) is divergent for $L \rightarrow \infty$ if $s \geq 2t + 1$. This is the case for stretched tubes, $\epsilon > 0$, where we have $s \in \{1, 2\}$ and $t = 0$. The integral is then straightforwardly evaluated with strain dependent coefficients ξ_1 and ξ_2 , yielding the long-tube scaling relations as described in Fig. 6.

-
- [1] A. A. Balandin, S. Ghosh, W. Bao, I. Calizo, D. Teweldebrhan, F. Miao, and C. N. Lau, Superior Thermal Conductivity of Single-Layer Graphene, *Nano Lett.* **8**, 902 (2008).
 - [2] E. Pop, D. Mann, Q. Wang, K. Goodson, and H. Dai, Thermal Conductance of an Individual Single-Wall Carbon Nanotube above Room Temperature, *Nano Lett.* **6**, 96 (2006), [arXiv:0512624 \[cond-mat\]](#).
 - [3] A. M. Marconnet, N. Yamamoto, M. A. Panzer, B. L. Wardle, and K. E. Goodson, Thermal Conduction in Aligned Carbon Nanotube–Polymer Nanocomposites with High Packing Density, *ACS Nano* **5**, 4818 (2011).
 - [4] K. M. F. Shahil and A. A. Balandin, Graphene–Multilayer Graphene Nanocomposites as Highly Efficient Thermal Interface Materials, *Nano Lett.* **12**, 861 (2012).
 - [5] Z. Yan, G. Liu, J. M. Khan, and A. A. Balandin, Graphene quilts for thermal management of high-power GaN transistors, *Nat. Commun.* **3**, 827 (2012).
 - [6] I. Kholmanov, J. Kim, E. Ou, R. S. Ruoff, and L. Shi, Continuous Carbon Nanotube–Ultrathin Graphite Hybrid Foams for Increased Thermal Conductivity and Suppressed Subcooling in Composite Phase Change Materials, *ACS Nano* **9**, 11699 (2015).
 - [7] P. Liu, Z. Fan, A. Mikhalech, T. Q. Tran, D. Jewell, H. M. Duong, and A. M. Marconnet, Continuous Carbon Nanotube-Based Fibers and Films for Applications Requiring Enhanced Heat Dissipation, *ACS Appl. Mater. Interfaces* **8**, 17461 (2016).
 - [8] W. Dai, T. Ma, Q. Yan, J. Gao, X. Tan, L. Lv, H. Hou, Q. Wei, J. Yu, J. Wu, Y. Yao, S. Du, R. Sun, N. Jiang, Y. Wang, J. Kong, C. Wong, S. Maruyama, and C.-T. Lin, Metal-Level Thermally Conductive yet Soft Graphene Thermal Interface Materials, *ACS Nano* **13**, 11561 (2019).
 - [9] A. A. Balandin, Thermal properties of graphene and nanostructured carbon materials, *Nat. Mater.* **10**, 569 (2011).

- [10] A. A. Balandin, Phononics of Graphene and Related Materials, *ACS Nano* **14**, 5170 (2020).
- [11] C. H. Xu, C. Z. Wang, C. T. Chan, and K. M. Ho, Theory of the thermal expansion of Si and diamond, *Phys. Rev. B* **43**, 5024 (1991).
- [12] N. Mounet and N. Marzari, First-principles determination of the structural, vibrational and thermodynamic properties of diamond, graphite, and derivatives, *Phys. Rev. B* **71**, 205214 (2005).
- [13] K. D. Parrish, A. Jain, J. M. Larkin, W. A. Saidi, and A. J. H. McGaughey, Origins of thermal conductivity changes in strained crystals, *Phys. Rev. B* **90**, 235201 (2014).
- [14] A. Aghaei, K. Dayal, and R. S. Elliott, Anomalous phonon behavior of carbon nanotubes: First-order influence of external load, *J. Appl. Phys.* **113**, 023503 (2013).
- [15] A. J. H. McGaughey, A. Jain, and H.-Y. Kim, Phonon properties and thermal conductivity from first principles, lattice dynamics, and the Boltzmann transport equation, *J. Appl. Phys.* **125**, 011101 (2019).
- [16] N. Bonini, J. Garg, and N. Marzari, Acoustic Phonon Lifetimes and Thermal Transport in Free-Standing and Strained Graphene, *Nano Lett.* **12**, 2673 (2012).
- [17] G. Fugallo, A. Cepellotti, L. Paulatto, M. Lazzeri, N. Marzari, and F. Mauri, Thermal Conductivity of Graphene and Graphite: Collective Excitations and Mean Free Paths, *Nano Lett.* **14**, 6109 (2014).
- [18] A. Cepellotti and N. Marzari, Thermal Transport in Crystals as a Kinetic Theory of Relaxons, *Phys. Rev. X* **6**, 041013 (2016), arXiv:1603.02608.
- [19] N. Mingo and D. A. Broido, Length Dependence of Carbon Nanotube Thermal Conductivity and the “Problem of Long Waves”, *Nano Lett.* **5**, 1221 (2005).
- [20] D. Bruns, A. Nojeh, A. S. Phani, and J. Rottler, Heat transport in carbon nanotubes: Length dependence of phononic conductivity from the Boltzmann transport equation and molecular dynamics, *Phys. Rev. B* **101**, 195408 (2020).
- [21] L. Lindsay, D. A. Broido, and N. Mingo, Lattice thermal conductivity of single-walled carbon nanotubes: Beyond the relaxation time approximation and phonon-phonon scattering selection rules, *Phys. Rev. B* **80**, 125407 (2009).
- [22] L. Lindsay, D. A. Broido, and N. Mingo, Diameter dependence of carbon nanotube thermal conductivity and extension to the graphene limit, *Phys. Rev. B* **82**, 161402(R) (2010).
- [23] S.-Y. Yue, T. Ouyang, and M. Hu, Diameter Dependence of Lattice Thermal Conductivity of Single-Walled Carbon Nanotubes: Study from Ab Initio, *Sci. Rep.* **5**, 15440 (2015).
- [24] G. Barbalinardo, Z. Chen, H. Dong, Z. Fan, and D. Donadio, Ultrahigh convergent thermal conductivity of carbon nanotubes from comprehensive atomistic modeling, *Phys. Rev. Lett.* **127**, 025902 (2021).
- [25] V. N. Popov, V. E. Van Doren, and M. Balkanski, Elastic properties of single-walled carbon nanotubes, *Phys. Rev. B* **61**, 3078 (2000).
- [26] H. Suzuura and T. Ando, Phonons and electron-phonon scattering in carbon nanotubes, *Phys. Rev. B* **65**, 235412 (2002).
- [27] A. De Martino, R. Egger, and A. O. Gogolin, Phonon-phonon interactions and phonon damping in carbon nanotubes, *Phys. Rev. B* **79**, 205408 (2009), arXiv:0903.1771.
- [28] P. Gupta and A. Kumar, Phonons in chiral nanorods and nanotubes: A Cosserat-rod-based continuum approach, *Math. Mech. Solids* **24**, 3897 (2019).
- [29] L. Lindsay and D. A. Broido, Optimized Tersoff and Brenner empirical potential parameters for lattice dynamics and phonon thermal transport in carbon nanotubes and graphene, *Phys. Rev. B* **81**, 205441 (2010), arXiv:1003.2236.
- [30] A. A. Maradudin and A. E. Fein, Scattering of Neutrons by an Anharmonic Crystal, *Phys. Rev.* **128**, 2589 (1962).
- [31] L. Lindsay and D. A. Broido, Theory of thermal transport in multilayer hexagonal boron nitride and nanotubes, *Phys. Rev. B* **85**, 035436 (2012).
- [32] W. Li, J. Carrete, N. A. Katcho, and N. Mingo, ShengBTE: A solver of the Boltzmann transport equation for phonons, *Comput. Phys. Commun.* **185**, 1747 (2014).
- [33] E. Viola and A. Marzani, Exact analysis of wave motions in rods and hollow cylinders, in *Mechanical Vibration: Where do we Stand?*, edited by I. Elishakoff (Springer Vienna, Vienna, 2007) pp. 83–104.
- [34] L. Landau and E. Lifshitz, *Theory of Elasticity* (Pergamon, Oxford, 1986).
- [35] J. Ziman, *Electrons and Phonons* (Oxford University Press, Oxford, 1960).
- [36] E. Lifshitz and L. Pitaevski, in *Physical Kinetics*, Course of Theoretical Physics, Vol. 10 (Pergamon, Oxford, 1981) pp. 284–311.
- [37] Z. Rashid, L. Zhu, and W. Li, Effect of confinement on anharmonic phonon scattering and thermal conductivity in pristine silicon nanowires, *Phys. Rev. B* **97**, 075441 (2018).
- [38] G. Srivastava, *The Physics of Phonons* (Taylor & Francis, New York, 1990).
- [39] K. H. Michel, S. Costamagna, and F. M. Peeters, Theory of anharmonic phonons in two-dimensional crystals, *Phys. Rev. B* **91**, 134302 (2015).
- [40] S. G. and D. Kumar, Anomalous transport and phonon renormalization in a chain with transverse and longitudinal vibrations, *Phys. Rev. E* **82**, 011130 (2010).
- [41] X. Wang, M. Kaviani, and B. Huang, Phonon coupling and transport in individual polyethylene chains: a comparison study with the bulk crystal, *Nanoscale* **9**, 18022 (2017).
- [42] T. Pandey, C. A. Polanco, V. R. Cooper, D. S. Parker, and L. Lindsay, Symmetry-driven phonon chirality and transport in one-dimensional and bulk Ba₃N-derived materials, *Phys. Rev. B* **98**, 241405(R) (2018).
- [43] L. Lindsay, D. A. Broido, and N. Mingo, Flexural phonons and thermal transport in graphene, *Phys. Rev. B* **82**, 115427 (2010).
- [44] A. Cepellotti, G. Fugallo, L. Paulatto, M. Lazzeri, F. Mauri, and N. Marzari, Phonon hydrodynamics in two-dimensional materials, *Nat. Commun.* **6**, 6400 (2015).
- [45] A. Chernatynskiy and S. R. Phillpot, Evaluation of computational techniques for solving the Boltzmann transport equation for lattice thermal conductivity calculations, *Phys. Rev. B* **82**, 134301 (2010).
- [46] P. B. Allen, Improved Callaway model for lattice thermal conductivity, *Phys. Rev. B* **88**, 144302 (2013).
- [47] J. Ma, W. Li, and X. Luo, Examining the Callaway model for lattice thermal conductivity, *Phys. Rev. B* **90**, 035203 (2014).

- [48] M. Born and K. Huang, *Dynamical Theory of Crystal Lattices* (Oxford University Press, Oxford, 1954). [Rev. B 48, 6033 \(1993\)](#).
- [49] Y.-J. Han and P. G. Klemens, Anharmonic thermal resistivity of dielectric crystals at low temperatures, [Phys.](#)